# UAV-Aided Wireless Communication Designs With Propulsion Energy Limitations

Subin Eom, Hoon Lee, *Member, IEEE*, Junhee Park, and Inkyu Lee, *Fellow, IEEE*

***Abstract*—In this paper, we investigate wireless communication systems where an unmanned aerial vehicle (UAV) supports data transmissions of multiple ground nodes (GNs) while maneuvering over the operating area. The propulsion energy consumption of the UAV is taken into consideration in this system, thus the UAV should operate under the certain threshold of the velocity and the acceleration. We formulate the minimum average rate maximization problem and the energy efficiency (EE) maximization problem by jointly optimizing the trajectory, velocity, and acceleration of the UAV and the uplink transmit power at the GNs. As these problems are non-convex in general, the successive convex approximation (SCA) scheme is employed. To utilize this technique, the non-convex constraints are turned into proper convex approximations, and iterative algorithms are proposed which converge to a local optimal point. From the numerical results, it is demonstrated that the proposed algorithms outperform baseline schemes for both problems. Especially for the EE maximization problem, the proposed algorithm exhibits about 109% gain over the baseline scheme.**

***Index Terms*—UAV communication, trajectory optimization, throughput maximization, energy efficiency (EE).**

## I. Introduction

In RECENT years, unmanned aerial vehicles (UAVs) have received great attentions as a new communication entity in wireless networks and internet of things (IoT) applications [2], [3]. Dissimilar to conventional systems which communicate through the ground base stations (BSs) fixed at a given position [4], UAV-aided systems could be deployed to the area with various purposes. Moreover, for channels between the air and the ground, there is a high probability of forming the line-of-sight (LoS) communication links since the UAV is located high above users [5]–[7].

Exploiting these benefits, UAVs have been utilized to diverse wireless communication scenarios. In [8] and [9], a UAV operates as a mobile relay which helps the communication of ground nodes (GNs), when direct communication links between GNs are blocked. Different from the typical fixed relay protocols [10], [11], in this UAV-aided relaying system, the UAV can move toward to nearby the GNs to provide good channel conditions, and thus significantly improved performance can be obtained. The authors in [8] maximized the throughput of mobile relaying channels by optimizing the trajectory of the mobile relay and the transmit power at the source and the relay node. For the fixed relay trajectory, the work [9] addressed the secrecy rate maximization problem for the UAV-based relaying system with an external eavesdropper.

In addition, UAVs have been adopted to assist conventional terrestrial communication infrastructures [12]–[14]. For the disaster situation, UAVs were employed in [12] to recover malfunctioned ground infrastructure. The work in [13] examined a system where the UAV serves cell-edge users by jointly optimizing user partitioning, bandwidth allocation, and UAV's trajectory. Also, the flying computing cloudlets with UAVs were introduced to provide offloading opportunities to multiple users [14].

Furthermore, in wireless networks, the UAVs could act as mobile BSs [15]–[17]. The authors in [15] derived mathematical expressions for the optimum altitude of the UAVs that maximizes the coverage of the cellular network. Also, the trajectory optimization methods for mobile BSs were presented in [16] and [17]. Assuming that the GNs are located in a line, the minimum throughput performance was maximized in [16] by optimizing the position of a UAV on a straight line. This result was extended in [17] to a general scenario where multiple UAVs fly three-dimensional space to communicate with GNs via a time-division multiple access (TDMA). The joint optimization algorithms for the UAV transmit power, trajectory, and time allocation were provided in [17] to maximize the minimum throughput performance. However, these works did not involve the propulsion energy consumption necessary for practical UAV designs under the limited on-board energy situation [18].

By taking this issue into account, recent works [19]–[21] investigated energy efficiency (EE) of the UAV system. Different from conventional systems which consider only communication-related energy consumption [22], [23], the EE of the UAV should address the propulsion energy at the UAV additionally. The authors in [19] maximized the EE by controlling the turning radius of a UAV for mobile relay systems. Also, from the joint optimization of the trajectory, speed, and time allocation, both the spectrum efficiency and the EE were maximized in [20]. In [21], the propulsion energy consumed at the fixed-wing UAV was theoretically modeled, and the EE

Manuscript received March 22, 2019; revised July 2, 2019 and September 16, 2019; accepted November 4, 2019. Date of publication November 11, 2019; date of current version January 15, 2020. This work was supported by the National Research Foundation through the Ministry of Science, ICT, and Future Planning (MSIP), Korean Government under Grant 2017R1A2B3012316. This paper was presented in part at the IEEE International Conference on Communications, Kansas City, MO, USA, May 2018 [1]. The review of this article was coordinated by Dr. S. Misra. *(Corresponding author: Inkyu Lee.)*

S. Eom, J. Park, and I. Lee are with the School of Electrical Engineering, Korea University, Seoul 02841, South Korea (e-mail: esb777@korea.ac.kr; pjh0585@korea.ac.kr; inkyu@korea.ac.kr).

H. Lee is with the Department of Information and Communications Engineering, Pukyong National University, Busan 48513, South Korea (e-mail: hlee@pknu.ac.kr).

Digital Object Identifier 10.1109/TVT.2019.2952883

maximization of the UAV was studied which assumed a single GN scenario.

This paper investigates a wireless communication system where a fixed-wing UAV with limited propulsion energy serves as a BS receiving the uplink communication of multiple GNs. Such a system could be applied to wireless networking scenarios where terrestrial BSs are not available for collecting data from GNs, e.g. the outdoor IoT environment such as climate measurement and monitoring systems, and the military or disaster case where base stations are destroyed or unavailable. It is assumed that multiple GNs share the same frequency bands and the time resources, and thus they simultaneously transmit their uplink signals to the UAV. This uplink transmission protocol has been widely studied as multiple access channels (MAC) [24], [25]. Under this setup, we jointly optimize the uplink transmit power of the GNs and the UAV movement variable such as the trajectory, the velocity, and the acceleration, in order to deal with both the minimum rate maximization problem and the EE maximization problem.

The authors in [17] solved the minimum rate maximization problem without considering the propulsion energy constraint. Different from our multiple access scheme where information from other GNs is considered as interference, TDMA with user scheduling was assumed in [17]. For the EE maximization problem, since [19], [20] considered a relay with constant power and our work can be regarded as a generalization of the single GN system with constant transmit power in [21] to the multi-GN scenario, we need to deal with inter-node interference and the power control of GNs as well. Due to these issues, direct application of existing algorithms presented in [17], [19]–[21] to our problems is difficult.

To tackle our problem of interest, we first couple the trajectory variables and the uplink transmit power by introducing auxiliary variables. Since the equivalent problems are still difficult to solve, we employ the successive convex approximation (SCA) technique [26], [27] which successively addresses approximated convex problems of the original non-convex one. By presenting new convex surrogate functions for the non-convex constraints, we can jointly optimize the variables at each iteration. Then we propose efficient algorithms for both the minimum rate maximization problem and the EE maximization problem. The convergence analysis of the proposed algorithms is also derived, and it is guaranteed that we can obtain at least locally optimum solutions. Based on the proposed algorithms, practical circular UAV trajectory is addressed. Simulation results confirm that the proposed algorithms provide a significant performance gain over baseline schemes.

The rest of this paper is organized as follows: Section II explains the system model and the problem formulations for the UAV-aided communication systems. In Section III, the minimum rate maximization and the EE maximization algorithms are proposed. We examine the circular trajectory case as baseline schemes in Section IV. Section V presents the numerical results for the proposed algorithms and in Section VI, we conclude the paper.

*Notations*: In this paper, we denote scalars and vectors as the normal and bold lower-case letters, respectively. For a vector $\mathbf{x}$, $\mathbf{x}^\intercal$ and $\|\mathbf{x}\|$ mean transpose and norm, respectively. $\mathbb{R}^{M\times 1}$ stands for the space of $M$-dimensional real-valued vectors. $\nabla f$ denotes the gradient of a function $f$.

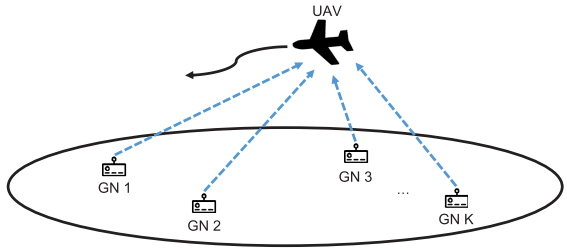


Fig. 1. A UAV-enabled wireless network system.

## II. System Model and Problem Formulation

In this paper, we consider a wireless communication system where a UAV receives information transmitted from $K$ GNs as depicted in Fig. 1. The system model is explained in Section II-A, and then it is followed by the problem formulations in Section II-B.

### A. System Model

As shown in Fig. 1, the UAV aviate on a constant altitude $H$ over the area of interest during a time period $T$, and the GNs operate at the fixed positions, where the UAV is aware of beforehand. In order to describe the location of the GNs and the UAV, a three-dimensional Cartesian coordinate system is adopted, and thus the horizontal coordinate of GN $k$ $(k = 1, \ldots, K)$ is expressed as $\mathbf{w}_k \in \mathbb{R}^{2\times 1}$. Also, by discretizing the time period $T$ into evenly divided $N$ time slots with duration $\delta_t = \frac{T}{N}$, the horizontal coordinate of the UAV at slot $n$ is represented as $\mathbf{q}[n] \in \mathbb{R}^{2\times 1}$ for $n = 0, 1, \ldots, N$[8]. Thus, the distance between GN $k$ and the UAV at $n$ slot is denoted by

$$d_k[n] = \sqrt{\|\mathbf{q}[n] - \mathbf{w}_k\|^2 + H^2}. \tag{1}$$

For the channel model between the GNs and the UAV, from the measurement data in [5], the LoS probability of air-to-ground communication links exceeds $95\%$ for our simulation setup. Based on this experimental work, it can be assumed that the LoS links are dominant over the air-to-ground communication links. Also, the Doppler effect arisen from the UAV's maneuverability is assumed to be well nullified. Then, the effective channel gain $h_k[n]$ from GN $k$ to the UAV can be derived following the free-space path loss model as [17], [21]

$$h_k[n] = \frac{\gamma_0}{d_k^2[n]}, \tag{2}$$

where $\gamma_0 \triangleq \beta_0/\sigma^2$ denotes the reference signal-to-noise ratio (SNR) at 1 m with $\sigma^2$ and $\beta_0$ being the white Gaussian noise power at the UAV and the channel power at 1 m, respectively.

For the uplink transmission, it is assumed that multiple GNs share the same frequency band and the time resource. The GNs transmit the information signals to the UAV at the same time, and thus the UAV suffers from the multi-user interference for decoding the message of each GN. At time slot $n$, GN $k$ sends

its information to the UAV with transmitting power $0 \le p_k[n] \le P_{\text{peak}}$, where $P_{\text{peak}}$ represents the peak power of the GNs. So, we can express the instantaneous achievable rate $R_k[n]$ as

$$R_k[n] = \log_2\left(1 + \frac{p_k[n]h_k[n]}{1 + \sum_{j=1, j\neq k}^{K} p_j[n]h_j[n]}\right), \quad (3)$$

where $\sum_{j=1,j\neq k}^{K} p_j[n]h_j[n]$ stands for interference from other GNs. Therefore, the achievable average rate of the GN $k$ and the total information bits transmitted from GN $k$ over $N$ time slots are denoted as $\frac{1}{N}\sum_{n=1}^{N} R_k[n]$ and $W\delta_t \sum_{n=1}^{N} R_k[n]$, respectively, where $W$ means the bandwidth.

For the power consumption of the UAV, the propulsion power which is used for keeping the UAV aloft and controlling its maneuverability is taken into account. In [21], the propulsion power consumption model of fixed-wing UAV was theoretically derived. For ease of analysis, the upper bound of this model is adopted, and we have

$$P_{\text{prop}}[n] = c_1\|\mathbf{v}[n]\|^3 + \frac{c_2}{\|\mathbf{v}[n]\|}\left(1 + \frac{\|\mathbf{a}[n]\|^2}{g^2}\right), \quad (4)$$

for $n = 0, 1, \ldots, N$, where $g = 9.8$ m/sec$^2$ equals the gravitational acceleration, $c_1$ and $c_2$ are the aircraft design related constants, and $\mathbf{v}[n]$ and $\mathbf{a}[n]$ are the velocity and the acceleration of the UAV at time slot $n$, respectively. Thus, we can obtain the average propulsion power and the total consumed propulsion energy over $N$ time slots as $\frac{1}{N}\sum_{n=1}^{N} P_{\text{prop}}[n]$ and $\delta_t \sum_{n=1}^{N} P_{\text{prop}}[n]$, respectively. We disregard the power consumption from the circuits for signal processing such as channel decoders and analog-to-digital converters, because they are practically much smaller than the propulsion power. [21].

Moreover, the restrictions on the UAV motion are expressed by using the movement variables as [21]

$$\mathbf{v}[n] = \mathbf{v}[n-1] + \mathbf{a}[n-1]\delta_t, \quad \forall n, \quad (5)$$

$$\mathbf{q}[n] = \mathbf{q}[n-1] + \mathbf{v}[n-1]\delta_t + \frac{1}{2}\mathbf{a}[n-1]\delta_t^2, \quad \forall n, \quad (6)$$

$$\mathbf{q}[0] = \mathbf{q}[N], \mathbf{v}[0] = \mathbf{v}[N], \mathbf{a}[0] = \mathbf{a}[N], \quad \forall n, \quad (7)$$

$$\|\mathbf{a}[n]\| \le a_{\max}, \quad \forall n, \quad (8)$$

$$V_{\min} \le \|\mathbf{v}[n]\| \le V_{\max}, \quad \forall n, \quad (9)$$

where $a_{\max}$ stands for the maximum UAV acceleration in m/sec$^2$ and $V_{\min}$ and $V_{\max}$ indicate the minimum and the maximum UAV speed in m/sec, respectively. Constraints (5) and (6) mean the relationship between the UAV movement variables, and (7) implies that after one period $T$, the UAV returns to its initial position with the same mobility, for supporting the GNs periodically [17]. Also, it is noticed that for practical fixed-wing UAV designs, the minimum speed constraint $V_{\min}$ is important since it allows the UAV to remain aloft. Thus, the UAV cannot hover over a fixed location.

### *B. Problem Formulation*

In this paper, the minimum average rate in multiple GNs and the EE are maximized, respectively, from the joint optimization of the uplink transmit power $p_k[n]$ at the GNs and the variables $\mathbf{q}[n]$, $\mathbf{v}[n]$, and $\mathbf{a}[n]$. First, we can formulate the minimum rate maximization problem as

$$(P1): \max_{\substack{\{\mathbf{q}[n],\mathbf{v}[n],\mathbf{a}[n]\}\\ \{p_k[n],\tau\}}} \quad \tau \quad (10a)$$

$$\text{s.t.} \quad \frac{1}{N}\sum_{n=1}^{N} R_k[n] \ge \tau, \quad \forall k, \quad (10b)$$

$$0 \le p_k[n] \le P_{\text{peak}}, \quad \forall k, n, \quad (10c)$$

$$\frac{1}{N}\sum_{n=1}^{N} P_{\text{prop}}[n] \le P_{\text{lim}}, \quad (10d)$$

$$(5)\text{–}(9),$$

where an auxiliary optimization variable $\tau$ indicates the minimum average rate among multiple GNs and $P_{\text{lim}}$ denotes the average propulsion power budget of the UAV.

Next, to support all of the individual GNs, the fairness based EE [28], [29] is more suitable than the network-wise EE [22], [23]. Thus, we define the EE in the UAV-aided wireless communication systems as the ratio between the minimum information bits transmitted among the GNs and the total energy consumed at the UAV. Therefore, we have the EE maximization problem as

$$(P2): \max_{\substack{\{\mathbf{q}[n],\mathbf{v}[n],\mathbf{a}[n]\}\\ \{p_k[n],\eta\}}} \quad \frac{\eta}{\sum_{n=1}^{N} P_{\text{prop}}[n]} \quad (11a)$$

$$\text{s.t.} \quad W\sum_{n=1}^{N} R_k[n] \ge \eta, \quad \forall k, \quad (11b)$$

$$(5)\text{–}(9), (10\text{c}),$$

where an auxiliary variable $\eta$ denotes the minimum transmitted information bits among the GNs. In (9), the norm is a convex function and thus the set that satisfies $V_{\min} \le \|\mathbf{v}[n]\|$ is not a convex set, and in (10b), $p_k[n]h_k[n]$ in $R_k[n]$ is neither a convex nor concave function of $p_k[n]$ and $\mathbf{q}[n]$. Moreover, because of the non-convex term $\frac{1}{\|\mathbf{v}[n]\|}$ in $P_{\text{prop}}[n]$, (10d) becomes non-convex constraints, and the objective of (P2) is a non-convex fractional function with a non-concave numerator over a non-convex denominator. Hence, (P1) and (P2) are non-convex problems, and thus it is not easy to reformulate them into equivalent convex problems and highly difficult to obtain the globally optimal solutions since no general optimization framework is available [30].

In comparison to [17], we additionally deal with the propulsion power limit (10d) in the minimum rate maximization problem (P1) with different multiple access schemes. In addition, note that the EE maximization problem (P2) where assumed a multiple GN case can be regarded as a generalization of [21] which investigated only a single GN scenario with constant transmit power. Thus, the inter-node interference and the power control of GNs are needed to be managed as well.

## III. Proposed Algorithm

In this section, efficient iterative algorithms for solving (P1) and (P2) are proposed based on the SCA scheme. Although the

SCA framework has been adopted in [17], the optimality of such method is not guaranteed in general since that is based on alternating optimization for multiple variables. Also, the SCA technique used in [21] alone cannot guarantee the optimality of the generalized multi-GN EE maximization problem. By introducing auxiliary variables and formulating new convex surrogate functions, we can guarantee the locally optimum of the proposed algorithms. First, the minimum rate maximization problem (P1) is considered in Section III-A, and then it is followed by the EE maximization problem (P2) in Section III-B.

### A. Minimum Average Rate Maximization

To deal with the highly coupled variables $p_k[n]$ and $h_k[n]$, we apply the change of variables as

$$G_k[n] \triangleq p_k[n]h_k[n] = \frac{p_k[n]\gamma_0}{\|\mathbf{q}[n]-\mathbf{w}_k\|^2+H^2}, \quad \forall k,n, \quad (12)$$

where $G_k[n]$ is a new optimization variable. Then the peak power constraint (10c) becomes $0 \le G_k[n] \le G_{k,\max}[n], \quad \forall k,n$, where $G_{k,\max}[n] \triangleq P_{\text{peak}}h_k[n] = \frac{P_{\text{peak}}\gamma_0}{\|\mathbf{q}[n]-\mathbf{w}_k\|^2+H^2}$. Thus, we can rewrite the achievable rate $R_k[n]$ in (3) as

$$R_k[n] = \log_2\left(1+\sum_{m=1}^{K} G_m[n]\right) - \hat{R}_k[n], \quad (13)$$

where $\hat{R}_k[n] \triangleq \log_2(1+\sum_{j=1,j\neq k}^{K} G_j[n])$.

To tackle the non-convex velocity constraint (9) and the propulsion power constraint (10d), we introduce new auxiliary variables $\{V_{\text{I}}[n]\}$. Then, (P1) can be reformulated as

$$(P1.1):$$

$$\max_{\substack{\{\mathbf{q}[n],\mathbf{v}[n],\mathbf{a}[n]\}\\ \{G_k[n],V_{\text{I}}[n],\tau\}}} \quad \tau \quad (14a)$$

$$\text{s.t.} \ \frac{1}{N}\sum_{n=1}^{N}\left(\log_2\left(1+\sum_{m=1}^{K} G_m[n]\right) - \hat{R}_k[n]\right) \ge \tau, \ \forall k, \quad (14b)$$

$$0 \le G_k[n] \le G_{k,\max}[n], \quad \forall k,n, \quad (14c)$$

$$\frac{1}{N}\sum_{n=1}^{N} c_1\|\mathbf{v}[n]\|^3 + \frac{c_2}{V_{\text{I}}[n]} + \frac{c_2\|\mathbf{a}[n]\|^2}{g^2V_{\text{I}}[n]} \le P_{\text{lim}}, \quad (14d)$$

$$V_{\min} \le V_{\text{I}}[n], \quad \forall n, \quad (14e)$$

$$V_{\text{I}}^2[n] \le \|\mathbf{v}[n]\|^2, \quad \forall n, \quad (14f)$$

$$\|\mathbf{v}[n]\| \le V_{\max}, \quad \forall n, \quad (14g)$$

$$(5)-(8).$$

It is noted that the inequality constraint in (14f) holds with equality at the optimal point of (P1.1) because the feasible region corresponding to (14 d) can be enlarged by increasing $V_{\text{I}}[n]$ until $V_{\text{I}}[n] = \|\mathbf{v}[n]\|$. Thus, (P1.1) is regarded as the equivalent problem of (P1). By adopting the new auxiliary variables $\{V_{\text{I}}[n]\}$, constraints (14d) and (14e) are turned into convex. However (14b), (14c), and (14f) are still non-convex in general.

For tractable analysis of these constraints, we adopt the SCA algorithm. First, we can check that the constraint (14b) is composed with a difference of two concave functions. Therefore, by using the first-order Taylor approximation, we have the convex surrogate function $\hat{R}_k^{\text{ub}}[n]$ for $\hat{R}_k[n]$ as

$$\hat{R}_k^{\text{ub}}[n] \triangleq \hat{\Gamma}_k[n]\sum_{j=1,j\neq k}^{K}(G_{j,l+1}[n]-G_{j,l}[n]) + \log_2\left(1+\sum_{j=1,j\neq k}^{K} G_{j,l}[n]\right) \ge \hat{R}_k[n], \quad (15)$$

where $G_{k,l}[n]$ indicates a solution of $G_k[n]$, which is obtained at the $l$-th iteration of the SCA process and $\hat{\Gamma}_k[n] \triangleq \log_2 e/(1+\sum_{j=1,j\neq k}^{K} G_{j,l}[n])$. Next, we derive the following lemmas in order to obtain the surrogate functions of (14c) and (14f).

*Lemma 1:* Denoting $\{\mathbf{q}_l[n]\}$ as a solution for $\{\mathbf{q}[n]\}$ calculated at the $l$-th iteration, we have the concave surrogate function $G_{k,\max}^{\text{lb}}[n]$ for $G_{k,\max}[n]$ as

$$G_{k,\max}^{\text{lb}}[n] \triangleq P_{\text{peak}}\gamma_0\Big(-\frac{\|\mathbf{q}_{l+1}[n]-\mathbf{w}_k\|^2}{H^4} + B_k[n](\mathbf{q}_{l+1}[n]-\mathbf{w}_k)^{\text{T}}(\mathbf{q}_l[n]-\mathbf{w}_k) + C_k[n]\Big) \le G_{k,\max}[n], \quad (16)$$

where the constants $B_k[n]$ and $C_k[n]$ are respectively represented as

$$B_k[n] \triangleq 2\left(\frac{1}{H^4} - \frac{1}{\left(\|\mathbf{q}_l[n]-\mathbf{w}_k\|^2+H^2\right)^2}\right),$$

$$C_k[n] \triangleq \frac{1}{\|\mathbf{q}_l[n]-\mathbf{w}_k\|^2+H^2} + \frac{2\|\mathbf{q}_l[n]-\mathbf{w}_k\|^2}{\left(\|\mathbf{q}_l[n]-\mathbf{w}_k\|^2+H^2\right)^2} - \frac{\|\mathbf{q}_l[n]-\mathbf{w}_k\|^2}{H^4}.$$

*Proof:* Please refer to Appendix A. ■

*Lemma 2:* The concave surrogate function of $\|\mathbf{v}_{l+1}[n]\|^2$ based on a solution $\{\mathbf{v}_l[n]\}$ obtained at the $l$-th iteration can be computed as

$$-\|\mathbf{v}_{l+1}[n]\|^2 + 2\mathbf{v}_l^{\text{T}}(2\mathbf{v}_{l+1}[n]-\mathbf{v}_l[n]) \le \|\mathbf{v}_{l+1}[n]\|^2. \quad (17)$$

*Proof:* Applying a similar process in Appendix A, we can conclude that the function in (17) satisfies the conditions for a concave surrogate function [26], [27]. ■

From Lemmas 1 and 2, different from the way in [17] which is based on alternating optimization for multiple variables, we can jointly optimize the power and the trajectory variables at each iteration. Also, these make the additional inter-node interference and the power control possible which are not addressed in [21]. So, at the $(l+1)$-th iteration, the non-convex constraints in (14c) and (14f) are turned into convex constraints as

$$0 \le G_{k,l+1}[n] \le G_{k,\max}^{\text{lb}}[n], \quad (18)$$

$$V_{\text{I}}^2[n] \le -\|\mathbf{v}_{l+1}[n]\|^2 + 2\mathbf{v}_l^{\text{T}}(2\mathbf{v}_{l+1}[n]-\mathbf{v}_l[n]). \quad (19)$$

**Algorithm 1:** Proposed Algorithm for (P1).

Initialize $\{\mathbf{q}_0[n], \mathbf{v}_0[n], G_{k,0}[n]\}, \quad \forall k, n$ and let $l = 0$.
**Repeat**
  Compute $\{\mathbf{q}_{l+1}[n], \mathbf{v}_{l+1}[n], G_{k,l+1}[n]\}$ for (P1.2) with given $\{\mathbf{q}_l[n], \mathbf{v}_l[n], G_{k,l}[n]\}$.
  Update $l \leftarrow l + 1$.
**Until** Convergence.
Obtain $p_k[n] = \frac{G_{k,l+1}[n]}{h_{k,l+1}[n]}$.

Therefore, with obtained solutions $\{\mathbf{q}_l[n], \mathbf{v}_l[n], G_{k,l}[n]\}$, the following problem at the $(l+1)$-th iteration of the SCA procedure is solved.

$(P1.2)$ :

$$\max_{\substack{\{\mathbf{q}_{l+1}[n],\mathbf{v}_{l+1}[n],\mathbf{a}[n]\}\\ \{G_{k,l+1}[n],V_1[n],\tau^{\text{lb}}\}}} \quad \tau^{\text{lb}} \tag{20a}$$

$$\text{s.t.} \quad \frac{1}{N}\sum_{n=1}^{N}\left(\log_2\left(1+\sum_{m=1}^{K} G_{m,l+1}[n]\right) - \hat{R}_k^{\text{ub}}[n]\right) \geq \tau^{\text{lb}}, \quad \forall k, \tag{20b}$$

$$(5)\text{–}(8), (14\text{d}), (14\text{e}), (14\text{g}), (18), (19),$$

where $\tau^{\text{lb}}$ denotes the lower bound of $\tau$ in the problem (P1). Because all constraints are turned into convex in (P1.2), the optimal solution of (P1.2) can be obtained via existing convex optimization solvers, e.g. CVX [31]. Based on these results, we summarize the proposed iterative procedure in Algorithm 1.

For the convergence analysis of Algorithm 1, let us define the objective values of (P1) and (P1.2) at the $l$-th iteration as $\tau_l$ and $\tau_l^{\text{lb}}$, respectively. Then we can express the relationship

$$\tau_l \;=\; \tau_l^{\text{lb}} \;\leq\; \tau_{l+1}^{\text{lb}} \leq\; \tau_{l+1}, \tag{21}$$

where the first equation holds because the surrogate functions in (15), (16), and (17) are tight at the given local points, the second inequality is derived from the non-decreasing property of the optimal solution of (P1.2), and the third inequality follows from the fact that the approximation problem (P1.2) is a lower bound of the original problem (P1).

From (21), we can conclude that the objective value $\tau$ in (P1) is non-decreasing for every iterations of Algorithm 1. Since the objective value $\tau$ in (P1) has a finite upper bound value and at given local points, the surrogate functions in (15), (16), and (17) obtain the same gradients as their original functions, it can be verified that Algorithm 1 is guaranteed to converge to at least a locally optimal solution for (P1) [26], [27]. It can be noted that Algorithm 1 only deals with the convex problem (P1.2) at each iteration, and thus the overall complexity of the proposed algorithm is polynomial in the worst case.

### *B. Energy Efficiency Maximization*

In this subsection, we consider the EE maximization problem (P2). First, by applying (12)–(13), and introducing an auxiliary variable $\{V_1[n]\}$, (P2) can be transformed as

$(P2.1)$ :

$$\max_{\substack{\{\mathbf{q}[n],\mathbf{v}[n],\mathbf{a}[n]\}\\ \{G_k[n],V_1[n],\eta\}}} \quad \frac{\eta}{\sum_{n=1}^{N} c_1\|\mathbf{v}[n]\|^3 + \frac{c_2}{V_1[n]} + \frac{c_2\|\mathbf{a}[n]\|^2}{g^2 V_1[n]}} \tag{22a}$$

$$\text{s.t.} \quad W\sum_{n=1}^{N}\left(\log_2\left(1+\sum_{m=1}^{K} G_m[n]\right) - \hat{R}_k[n]\right) \geq \eta, \quad \forall k, \tag{22b}$$

$$(5)\text{–}(8), (14\text{c}), (14\text{e})\text{–}(14\text{g}).$$

Similar to (P1.1), we can see that (P2.1) is equivalent to (P2), but (P2.1) is still difficult to solve due to the non-convex constraints in (14c), (14f), and (22b).

To tackle this issue, we can employ the similar SCA process presented in Section III-A. By adopting (15) and Lemmas 1 and 2, a convex approximation of (P2.1) at the $(l+1)$-th iteration is given by

$(P2.2)$ :

$$\max_{\substack{\{\mathbf{q}_{l+1}[n],\mathbf{v}_{l+1}[n],\mathbf{a}[n]\}\\ \{G_{k,l+1}[n],V_1[n],\eta^{\text{lb}}\}}} \quad \frac{\eta^{\text{lb}}}{\sum_{n=1}^{N} c_1\|\mathbf{v}[n]\|^3 + \frac{c_2}{V_1[n]} + \frac{c_2\|\mathbf{a}[n]\|^2}{g^2 V_1[n]}} \tag{23a}$$

$$\text{s.t.} \quad W\sum_{n=1}^{N}\left(\log_2\left(1+\sum_{m=1}^{K} G_{m,l+1}[n]\right) - \hat{R}_k^{\text{ub}}[n]\right) \geq \eta^{\text{lb}}, \quad \forall k \tag{23b}$$

$$(5)\text{–}(8), (14\text{e}), (14\text{g}), (18), (19),$$

where $\eta^{\text{lb}}$ denotes the lower bound of $\eta$ in the original problem (P2).

It can be shown that (P2.2) is a concave-convex fractional problem, so we can optimally solve (P2.2) via the Dinkelbach's method [32], [33]. Then, denoting $\mu = \sum_{n=1}^{N} c_1\|\mathbf{v}[n]\|^3 + \frac{c_2}{V_1[n]} + \frac{c_2\|\mathbf{a}[n]\|^2}{g^2 V_1[n]}$ with a given constant $\lambda_m$, (P2.2) can be converted to (P2.3) as

$(P2.3)$ :

$$\max_{\substack{\{\mathbf{q}_{l+1}[n],\mathbf{v}_{l+1}[n],\mathbf{a}[n]\}\\ \{G_{k,l+1}[n],V_1[n],\eta^{\text{lb}}\}}} \quad \eta^{\text{lb}} - \lambda_m\mu \tag{24a}$$

$$\text{s.t.} \quad (5)\text{–}(8), (14e), (14g), (18), (19), (23b).$$

Based on (P2.3), we summarize the proposed iterative procedure in Algorithm 2. The convergence and the local optimality of Algorithm 2 can be verified similar to Algorithm 1, and thus the details are omitted for brevity.

It is worthwhile to note that the initialization of the trajectory variables $\{\mathbf{q}[n], \mathbf{v}[n]\}$ for (P1) and (P2) is needed. However, it is not trivial to find such variables satisfying the UAV movement constraints (5)–(9) and the propulsion power constraint (10d). This will be clearly explained in Section IV-C.

**Algorithm 2:** Proposed Algorithm for (P2).

Initialize $\{\mathbf{q}_0[n], \mathbf{v}_0[n], G_{k,0}[n]\}, \quad \forall k, n$ and let $\lambda_0 = 0$, $m = 0$, and $l = 0$.
**Repeat**
  **Repeat**
    Compute $\{\mathbf{q}_{l+1}[n], \mathbf{v}_{l+1}[n], G_{k,l+1}[n]\}$ for (P2.3) with given $\{\mathbf{q}_l[n], \mathbf{v}_l[n], G_{k,l}[n]\}, \quad \forall k, n$ and $\lambda_m$.
    Update $l \leftarrow l + 1$.
  **Until** Convergence
  Let $F(\lambda_m) = \eta^{\text{lb}} - \lambda_m \mu$ and $\lambda_{m+1} = \eta^{\text{lb}}/\mu$.
  Update $m \leftarrow m + 1$.
  Let $\{\mathbf{q}_0[n], \mathbf{v}_0[n], G_{k,0}[n]\}$
    $= \{\mathbf{q}_{l+1}[n], \mathbf{v}_{l+1}[n], G_{k,l+1}[n]\}, \quad \forall k, n$ and $l = 0$.
**Until** Convergence
Obtain $p_k[n] = \frac{G_{k,l+1}[n]}{h_{k,l+1}[n]}, \quad \forall k, n$.

## IV. Circular Trajectory System

Now, we examine practical optimization approaches for the fixed-wing UAV by restricting the travelling path of the UAV to a circular shape. First, (P1) and (P2) are converted for the circular trajectory in Section IV-A, and the circular trajectory optimization algorithms are given in Section IV-B. Section IV-C discusses initialization schemes for the proposed algorithms.

### A. Problem Formulation for the Circular Trajectory

First, we choose the center of the circular trajectory $\mathbf{c} = [x_0 \ y_0]^\intercal$ as the geometrical mean of the GNs $\mathbf{c} = \frac{\sum_{k=1}^{K} \mathbf{w}_k}{K}$. Denoting $r$ as the radius of the trajectory and $\theta[n]$ as the angle of the circle along which the UAV flies at time slot $n$, the horizontal coordinate of the UAV $\mathbf{q}[n]$ can be obtained by $\mathbf{q}[n] = [r\cos\theta[n] + x_0 \ r\sin\theta[n] + y_0]^\intercal$. Also, the location of GN $k$ $\mathbf{w}_k$ can be represented as $\mathbf{w}_k = [\zeta_k \cos\varphi_k + x_0 \ \ \zeta_k \sin\varphi_k + y_0]^\intercal$, where $\zeta_k$ and $\varphi_k$ equal the distance and the angle between the geometric center $\mathbf{c}$ and GN $k$, respectively. Thus, the distance $d_k[n]$ between the UAV and GN $k$ in (1) can be expressed as $d_k[n] = \sqrt{r^2 + \zeta_k^2 + H^2 - 2r\zeta_k \cos(\theta[n] - \varphi_k)}$.

Different from the simple circular trajectory systems which assumed constant velocity [19]–[21], we adopt the angular velocity $\omega[n]$ and the angular acceleration $\alpha[n]$ and thus equations in (4)–(9) can be rewritten as

$$P_{\text{prop}}[n] = c_1 r^3 \omega^3[n] + \frac{c_2}{r\omega[n]} + \frac{c_2 r\omega^3[n]}{g^2} + \frac{c_2 r\alpha^2[n]}{g^2\omega[n]}, \quad \text{for } n = 0, 1, \ldots, N, \tag{25}$$

$$\omega[n] = \omega[n-1] + \alpha[n-1]\delta_t, \ \text{for } n = 1, \ldots, N, \tag{26}$$

$$\theta[n] = \theta[n-1] + \omega[n-1]\delta_t + \frac{1}{2}\alpha[n-1]\delta_t^2, \quad \text{for } n = 1, \ldots, N, \tag{27}$$

$$\theta[N] = \theta[0] + 2\pi, \omega[0] = \omega[N], \alpha[0] = \alpha[N], \tag{28}$$

$$\|\mathbf{a}[n]\|^2 = \|\mathbf{a}_{\parallel}[n]\|^2 + \|\mathbf{a}_{\perp}[n]\|^2 = r^2\alpha^2[n] + r^2\omega^4[n] \le a_{\max}^2, \ \text{for } n = 0, 1, \ldots, N, \tag{29}$$

$$\omega_{\min} \le \omega[n] \le \omega_{\max}, \ \text{for } n = 0, 1, \ldots, N, \tag{30}$$

where $\mathbf{a}_{\parallel}[n]$ and $\mathbf{a}_{\perp}[n]$ are the tangential and centripetal accelerations, respectively, and $\omega_{\min} \triangleq V_{\min}/r$ and $\omega_{\max} \triangleq V_{\max}/r$ indicate the minimum and maximum angular velocity, respectively.

Similar to Section III, we address the minimum average rate maximization problem and the EE maximization problem for the circular trajectory, which are respectively formulated as

$$(P3): \max_{\substack{\{\theta[n],\omega[n],\alpha[n]\} \\ \{r,p_k[n],\tau\}}} \quad \tau \tag{31a}$$

$$\text{s.t.} \quad r_{\min} \le r \le r_{\max}, \tag{31b}$$

$$(10\text{b})\text{–}(10\text{d}), (26)\text{–}(30),$$

$$(P4): \max_{\substack{\{\theta[n],\omega[n],\alpha[n]\} \\ \{r,p_k[n],\eta\}}} \frac{\eta}{\sum_{n=1}^{N} P_{\text{prop}}[n]} \tag{32a}$$

$$\text{s.t.} \quad (10\text{c}), (11\text{b}), (26)\text{–}(30), (31\text{b}),$$

where $r_{\min} \triangleq \frac{V_{\min}T}{2\pi}$ and $r_{\max} \triangleq \min\left(\frac{V_{\max}T}{2\pi}, \frac{a_{\max}}{\max\sqrt{\omega^4[n] + \alpha^2[n]}}\right)$ denote the minimum and maximum radius of the circular trajectory, respectively. It is emphasized that (P3) and (P4) are difficult to solve because of the non-convex constraints and objective functions. To deal with the problems (P3) and (P4), similar SCA frameworks in Section III are applied.

### B. Minimum Average Rate Maximization and EE Maximization

For the minimum average rate maximization problem (P3), we first find $\{r, p_k[n]\}$ with given $\{\theta[n], \omega[n], \alpha[n]\}$ and then updates $\{\theta[n], \omega[n], \alpha[n], p_k[n]\}$ for a fixed $r$. For given $\{\theta[n], \omega[n], \alpha[n]\}$, we adopt the change of variable $S_k[n]$ and $S_{k,\max}[n]$ as

$$S_k[n] \triangleq p_k[n]h_k[n] = \frac{p_k[n]\gamma_0}{(r - \zeta_k\cos(\theta[n] - \theta_k))^2 + \zeta_k^2\sin^2(\theta[n] - \theta_k) + H^2}, \tag{33}$$

$$S_{k,\max}[n] \triangleq P_{\text{peak}}h_k[n] = \frac{P_{\text{peak}}\gamma_0}{(r - \zeta_k\cos(\theta[n] - \theta_k))^2 + \zeta_k^2\sin^2(\theta[n] - \theta_k) + H^2}. \tag{34}$$

Similar to the method in Section III-A, we employ the SCA to $S_{k,\max}[n]$. Based on Lemma 1, the concave surrogate function $S_{k,\max}^{\text{lb1}}[n]$ of $S_{k,\max}[n]$ with a solution $r_l$ at the $l$-th iteration can be chosen as

$$S_{k,\max}^{\text{lb1}}[n] \triangleq P_{\text{peak}}\gamma_0\Big(-\frac{\left(r_{l+1} - \check{b}_k[n]\right)^2}{\check{A}_k^2[n]} + \check{B}_k[n]\left(r_{l+1} - \check{b}_k[n]\right)\left(r_l - \check{b}_k[n]\right) + \check{C}_k[n]\Big) \le S_{k,\max}[n], \quad \forall n, \tag{35}$$

where the constants $\check{b}_k[n]$, $\check{A}_k[n]$, $\check{B}_k[n]$, and $\check{C}_k[n]$ are respectively given by

$$\check{b}_k[n] \triangleq \zeta_k \cos\left(\theta[n]-\theta_k\right),$$

$$\check{A}_k[n] \triangleq \zeta_k^2 \sin^2\left(\theta[n]-\theta_k\right)+H^2,$$

$$\check{B}_k[n] \triangleq 2\left(\frac{1}{\check{A}_k^2[n]}-\frac{1}{\left(\left(r_l-\check{b}_k[n]\right)^2+\check{A}_k[n]\right)^2}\right),$$

$$\check{C}_k[n] \triangleq \frac{1}{\left(r_l-\check{b}_k[n]\right)^2+\check{A}_k[n]}+\frac{2\left(r_l-\check{b}_k[n]\right)^2}{\left(\left(r_l-\check{b}_k[n]\right)^2+\check{A}_k[n]\right)^2}-\frac{\left(r_l-\check{b}_k[n]\right)^2}{\check{A}_k^2[n]}.$$

By applying (15), (P3) for fixed $\{\theta[n],\omega[n],\alpha[n]\}$ can be reformulated as an approximated convex problem at the $(l+1)$-th iteration

$(P3.1)$ :

$$\max_{\{r_{l+1},S_{k,l+1}[n],\tau^{\text{lb1}}\}} \quad \tau^{\text{lb1}} \tag{36a}$$

$$\text{s.t.} \quad \frac{1}{N}\sum_{n=1}^{N}\left(\log_2\left(1+\sum_{m=1}^{K}S_{m,l+1}[n]\right)-\breve{R}_k^{\text{ub}}[n]\right) \geq \tau^{\text{lb1}},\ \forall k, \tag{36b}$$

$$0 \leq S_k[n] \leq S_{k,\max}^{\text{lb1}}[n],\ \forall k,n, \tag{36c}$$

$$(10d),(31b),$$

where $\breve{R}_k^{\text{ub}}[n] \triangleq \breve{\Gamma}_k[n](\sum_{j=1,j\neq k}^{K}(S_{j,l+1}[n]-S_{j,l}[n]))+\log_2(1+\sum_{j=1,j\neq k}^{K}S_{j,l}[n])$ and $\breve{\Gamma}_k[n] \triangleq \log_2 e/(1+\sum_{j=1,j\neq k}^{K}S_{j,l}[n])$. (P3.1) can be successively solved by the CVX until convergence.

Next, we present a solution for (P3) with a given $r$. To obtain the concave surrogate function of $S_{k,\max}[n]$, we introduce the following lemma which identifies the surrogate function of the cosine function.

*Lemma 3:* For any given $\phi_l$, the concave surrogate function of $\cos\phi$ can be computed as

$$\frac{-(\phi-\phi_l+\sin\phi_l)^2}{2}+\cos\phi_l+\frac{\sin^2\phi_l}{2} \leq \cos\phi. \tag{37}$$

*Proof:* With a similar process in Appendix A, we can conclude that the function in (37) satisfies the conditions for a concave surrogate function [26], [27]. ■

By inspecting Lemmas 1 and 3, the concave surrogate function $S_{k,\max}^{\text{lb2}}[n]$ for $S_{k,\max}[n]$ can be identified as

$$S_{k,\max}^{\text{lb2}}[n] \triangleq P_{\text{peak}}\gamma_0\Big(-\frac{r\zeta_k\left(\theta_{l+1}[n]-\hat{b}_k[n]\right)^2}{\hat{A}_k^2[n]} + \hat{B}_k[n]\sin(\theta_l[n]-\theta_k)\left(\theta_{l+1}[n]-\hat{b}_k[n]\right)+\hat{C}_k[n]\Big) \leq \frac{P_{\text{peak}}\gamma_0}{r\zeta_k\left(\theta_{l+1}[n]-\hat{b}_k[n]\right)^2+\hat{A}_k[n]} \leq S_{k,\max}[n], \tag{38}$$

where $\hat{b}_k[n]$, $\hat{A}_k[n]$, $\hat{B}_k[n]$, and $\hat{C}_k[n]$ are respectively obtained by

$$\hat{b}_k[n] \triangleq \theta_l[n]-\sin\left(\theta_l[n]-\theta_k\right),$$

$$\hat{A}_k[n] \triangleq r^2+\zeta_k^2+H^2 - r\zeta_k\left(2\cos\left(\theta_l[n]-\theta_k\right)+\sin^2\left(\theta_l[n]-\theta_k\right)\right),$$

$$\hat{B}_k[n] \triangleq 2r\zeta_k\left(\frac{1}{\hat{A}_k^2[n]}-\frac{1}{\left(r\zeta_k\sin^2(\theta_l[n]-\theta_k)+\hat{A}_k[n]\right)^2}\right),$$

$$\hat{C}_k[n] \triangleq \frac{1}{r\zeta_k\sin^2(\theta_l[n]-\theta_k)+\hat{A}_k[n]}+\frac{2r\zeta_k\sin^2(\theta_l[n]-\theta_k)}{\left(r\zeta_k\sin^2(\theta_l[n]-\theta_k)+\hat{A}_k[n]\right)^2}-\frac{r\zeta_k\sin^2(\theta_l[n]-\theta_k)}{\hat{A}_k^2[n]}.$$

By utilizing (15) and (38), at the $(l+1)$-th iteration of the SCA algorithm with a given $r$, (P3) can be approximated to the following convex problem.

$(P3.2)$ :

$$\max_{\substack{\{\theta_{l+1}[n],\omega[n],\alpha[n]\}\\ \{S_{k,l+1}[n],\tau^{\text{lb2}}\}}} \quad \tau^{\text{lb2}} \tag{39a}$$

$$\text{s.t.} \quad \frac{1}{N}\sum_{n=1}^{N}\left(\log_2\left(1+\sum_{m=1}^{K}S_{m,l+1}[n]\right)-\breve{R}_k^{\text{ub}}[n]\right) \geq \tau^{\text{lb2}}, \quad \forall k, \tag{39b}$$

$$0 \leq S_k[n] \leq S_{k,\max}^{\text{lb2}}[n], \quad \forall k,n, \tag{39c}$$

$$(10\text{d}),(26)\text{–}(30).$$

We then successively solve (P3.2) by the CVX until convergence. Similar to Algorithm 1, a solution of problem (P3) is obtained by alternately solving (P3.1) and (P3.2) until the objective value converges. For the EE maximization problem (P4) in the circular trajectory case, we can apply similar methods in Section III-B. Based on (P3.1) and (P3.2), given $\{\theta[n],\omega[n],\alpha[n]\}$ and $r$, (P4) can be transformed into two concave-convex fractional problems. By using Algorithm 2, we can alternately solve these problems until convergence.

### C. Trajectory Initialization

To initialize the proposed algorithms, we employ a simple circular path concept in [17]. First, the initial angular velocity $\omega_0$ is set to $\omega_0=\frac{2\pi}{T}$, which implies $\theta_0[n]=2\pi\frac{n}{N}, \quad \forall n$. Next, the initial radius $r_0$ is chosen to fulfill the constraints in (8), (9), and (10d), which can be expressed as

$$\frac{V_{\min}T}{2\pi} \leq r_0 \leq \min\left(\frac{V_{\max}T}{2\pi},\frac{a_{\max}}{\omega_0^2}\right), \tag{40}$$

$$c_1 r_0^3\omega_0^3+\frac{c_2}{r_0\omega_0}+\frac{c_2 r_0\omega_0^3}{g^2} \leq P_{\text{lim}}. \tag{41}$$

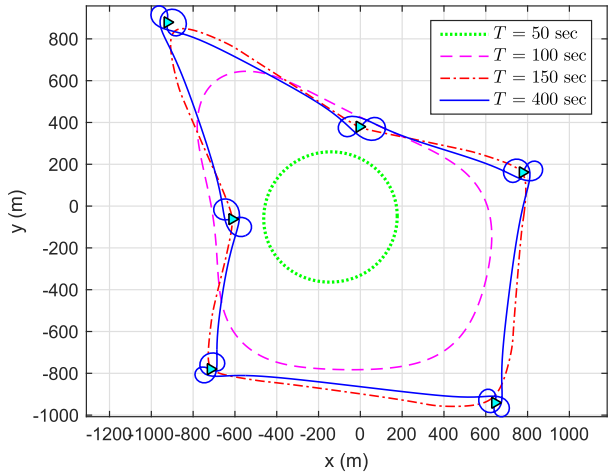


Fig. 2. Optimized UAV trajectories for different periods $T$ with $P_{\text{lim}} = 150$ W.

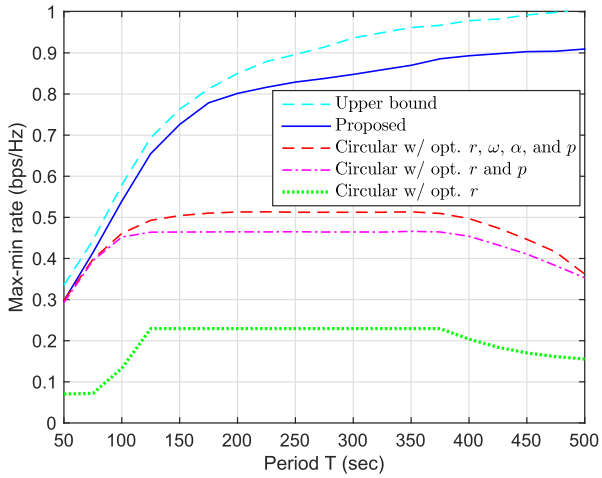


Fig. 3. Max-min rate with respect to the period $T$ with $P_{\text{lim}} = 150$ W.

We can simply find $r_0$ which maximizes the minimum rate in (P1) and (P3) under constraints (40) and (41) via one-dimensional line search. For the EE maximization problems (P2) and (P4), $r_0$ can be computed in the range of (40). As a result, the initial trajectory $\mathbf{q}_0[n]$ can be denoted by $\mathbf{q}_0[n] = [r_0 \cos 2\pi \frac{n}{N} + x_0 \quad r_0 \sin 2\pi \frac{n}{N} + y_0]^\intercal \ \ (n = 0, 1, \ldots, N)$ and the initial velocity $\mathbf{v}_0[n]$ can be simply obtained as $\mathbf{v}_0[n] = (\mathbf{q}_0[n+1] - \mathbf{q}_0[n])/\delta_t \ (n = 0, 1, \ldots, N-1)$ assuming $\delta_t^2 \approx 0$ in (6).

## V. Numerical Results

In this section, the effectiveness of the proposed algorithms is validated by numerical results.[1] We assume the rural area communication scenario and $K = 6$ GNs are spatially distributed in a wide square area of size $2 \times 2$ km$^2$, where the locations of the GNs are marked with the triangles in Fig. 2. The constant altitude, the bandwidth, the reference SNR, and the peak transmission power are set to be $H = 100$ m [5], $W = 1$ MHz, $\gamma_0 = 80$ dB, and $P_{\text{peak}} = 10$ dBm, respectively. Also, the minimum velocity, the maximum velocity, and the maximum acceleration of the UAV are determined as $V_{\min} = 3$ m/sec, $V_{\max} = 50$ m/sec, and $a_{\max} = 5$ m/sec$^2$, respectively [21]. For the UAV's propulsion power consumption model in (4), the constants $c_1$ and $c_2$ are set as $c_1 = 9.26 \times 10^{-4}$ and $c_2 = 2250$, respectively, which make the minimum propulsion power consumption $P_{\text{prop,min}} = 100$ W when $\|\mathbf{v}\| = 30$ m/sec [20], [21].

We first demonstrate the performance of the minimum rate maximization algorithms. For $P_{\text{lim}} = 150$ W case, the optimized UAV trajectories with various $T$ are depicted in Fig. 2. In the case of sufficiently large $T$ ($T = 400$ sec), the UAV is able to travel all the GNs during a given time period. Due to the constraints on the propulsion power and the velocity, the UAV cannot stop over constant location. Therefore, the UAV hovers over each GN by flying a smooth path around the GNs.

[1]The simulations are implemented in Matlab R2015a on a PC equipped with an Intel Core i7-4790 K 4.00 GHz processor and 16 GB of RAM.

Fig. 3 shows the maximized minimum (max-min) rate of the proposed algorithm as a function of $T$. We compare the performance of the proposed algorithm to the following upper bound and circular trajectory based methods [19], [20].

- *Upper bound*: Unachievable upper bound is calculated by bringing the assumptions in [17] to (P1) for an ideal case, where $V_{\min} = 0$, $a_{\max} \to \infty$, and $P_{\text{lim}} \to \infty$, i.e., when the hovering is possible for the UAV with infinite propulsion energy and no acceleration limit.
- *Circular with optimum* $r, \omega, \ \alpha$, *and* $p$: radius, angular velocity, angular acceleration, and uplink transmit power are jointly optimized with (P3) in Section IV-A with the circular trajectory.
- *Circular with optimum* $r$ *and* $p$: For circular trajectory, radius and uplink transmit power are jointly optimized with (P3.1) in Section IV-A, which can be considered as the methods in [19] and [20] with constant speed.
- *Circular with optimum* $r$: radius is optimized with $P_{\text{peak}}$ for all GNs as the initial circular trajectory in Section IV-C.

It is observed that except for the $T = 50$ sec case which is strongly bounded by the acceleration constraint, the UAV fully exploits given propulsion power limit $P_{\text{lim}}$ at the proposed trajectory. In addition, the performance of the proposed algorithm is superior to the baseline schemes for all the time period $T$. Furthermore, as the UAV can allocate more time to hover around each GN, the max-min rates obtained from the proposed algorithm and the upper bound increase monotonically as $T$ grows. On the contrast, for the baseline schemes with circular shape trajectory, the max-min rate performance increases in an early stage and decreases after saturation as $T$ grows. In the medium range of $T$, the optimal radius can be obtained satisfying the physical constraints on the circular shape path. Thus, the max-min rate performance does not change even if $T$ increases. However, in order to operate under the propulsion power budget, the radius of the circle which the UAV move on should increase as $T$ gets large, and thus the UAV may become too far away from the geometric center of the GNs after a certain $T$. Therefore, we can expect the performance gain of the proposed algorithm over baseline schemes is getting larger when $T$ grows.

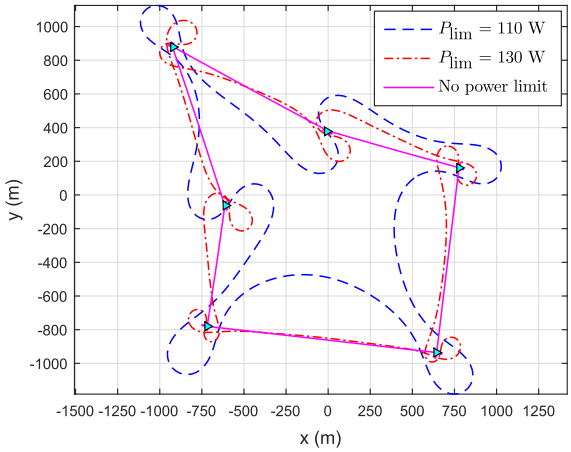


Fig. 4. Optimized UAV trajectories for different propulsion power limit $P_{\lim}$ with $T = 400$ sec.

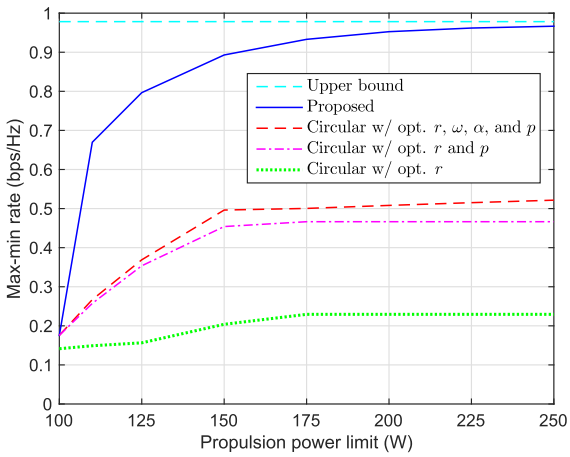


Fig. 5. Max-min rate with respect to the propulsion power limit $P_{\lim}$ with $T = 400$ sec.

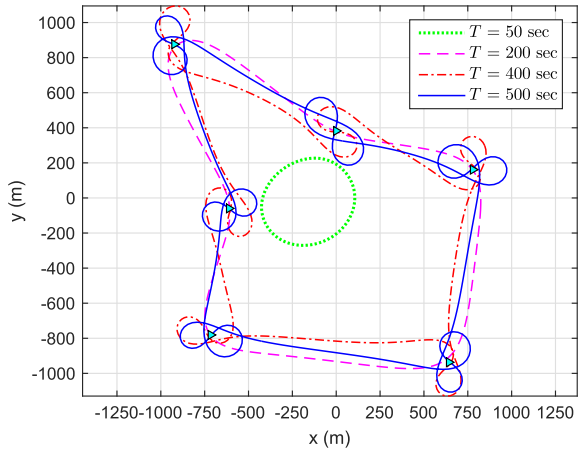


Fig. 6. Optimized energy efficient UAV trajectories for different periods $T$.

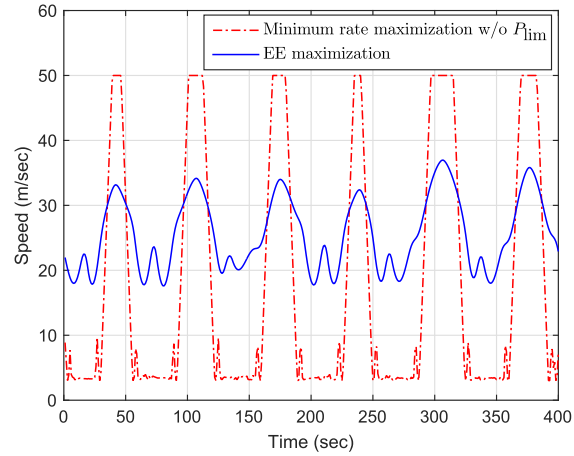


Fig. 7. UAV speeds for the max-min rate without propulsion power constraint and the EE maximization with $T = 400$ sec.

Fig. 4 illustrates the optimized UAV trajectories for various propulsion power limit $P_{\lim}$ with $T = 400$ sec. It can be shown that for $P_{\lim} = 110$ W, the trajectory of the UAV is restricted to a smooth path with a large turning radius to consume a low propulsion power. However, as $P_{\lim}$ gets larger, we observe quick changes along the trajectory path. Thus the UAV can move with a much smaller turning radius, which enhances the max-min rate performance.

In Fig. 5, we depict the average max-min rate of various schemes as a function of the propulsion power constraint $P_{\lim}$. For both the proposed algorithm and the baseline schemes, the max-min rate first increases as $P_{\lim}$ grows and then gets saturated. This can be explained as follows: With a large $P_{\lim}$, the trajectory and the velocity of the UAV change more freely to attain good channel conditions, and thus the max-min rate increases. However, even if a large $P_{\lim}$ is given, the max-min rate cannot continue to increase because there are practical limits on the velocity and acceleration. Thus, it is observed that the proposed algorithm shows a similar performance to the upper bound as $P_{\lim}$ grows. Similar to Fig. 3, we can see that the performance of the proposed algorithm achieves significant gain over the that of the baseline schemes.

Next, in Fig. 6, we investigate the optimized trajectory of the EE maximization problem with various $T$. As $T$ increases, the overall patterns are similar to Fig. 2. Nevertheless, to balance between the throughput performance and the propulsion power consumed at the UAV, the EE maximization trajectory shows a smooth path with a relatively large turning radius, and thus the average propulsion power consumption becomes lower.

To present the impact of the energy efficient UAV communication designs, Fig. 7 depicts the UAV speed of the proposed EE maximization method with $T = 400$ sec. For comparison, we also consider the max-min rate scheme without the propulsion power constraint based on Algorithm 1. We can see that for the max-min rate case, the UAV tries to fly between the GNs as fast as possible and stay over the GNs with a low speed. On the other hand, the EE maximization scheme keeps the speed of the UAV at around 30 m/sec in order not to waste the propulsion energy.

Table I presents the performance comparison of the max-min rate without propulsion power constraint and the EE maximization designs for both the proposed and the baseline schemes

TABLE I
PERFORMANCE COMPARISON WITH MAX-MIN RATE AND EE MAXIMIZATION FOR $T = 400$ SEC

| | | Average max-min rate (bps/Hz) | Average power (Watts) | Energy efficiency (kbits/Joule) |
|---|---|---|---|---|
| Max-min rate w/o $P_{\lim}$ | Proposed | 0.97 | 486.55 | 1.99 |
| | Circular | 0.54 | 545.44 | 0.99 |
| EE maximization | Proposed | 0.79 | 122.14 | 6.47 |
| | Circular | 0.47 | 151.33 | 3.10 |

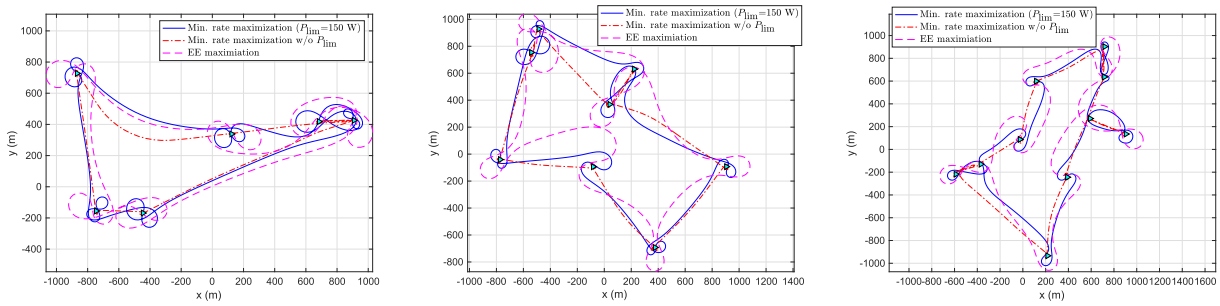


(a) $K = 6$ (b) $K = 8$ (c) $K = 10$

Fig. 8. Optimized UAV trajectories for different number of nodes with $T = 400$.

with $T = 400$ sec. It can be observed that the max-min rate methods consume much higher propulsion power by allowing a large variation of the speed and the average acceleration. In contrast, the speed of the proposed EE maximization design slowly varies with low acceleration, and thus much higher EE can be achieved. We observe that the proposed EE maximization algorithm exhibits about 225% gain over the max-min rate without the propulsion power constraint and 109% gain over the circular baseline EE maximization scheme.

Finally, to further verify the effectiveness of the proposed algorithms in more complicated setups, in Fig. 8, we depict the optimized trajectories for different network deployment scenarios with $K = 6, 8, 10$ and $T = 400$ sec. We can observe that the trajectories in Fig. 8 have a similar tendency to those given in Figs. 2, 4, and 6 regardless of the number of the GNs and their distribution. Also, the performance of the proposed algorithm is superior to that of the baseline schemes. For example, when $K = 8$ and $P_{\lim} = 150$ W, the max-min rate of the proposed algorithm and 'Circular w/ opt. $r$, $\omega$, $\alpha$, and $p$' is computed as 0.685 and 0.313 bps/Hz, respectively. For the EE maximization problem, the EE of the proposed algorithm is given by 5.08 kbits/Joule, while 'minimum rate maximization w/o $P_{\lim}$' and the circular trajectory method achieve 1.63 and 2.12 kbits/Joule, respectively. This indicates that the proposed algorithms still work well in more complicated deployment setups of the GNs.

## VI. CONCLUSION

In this paper, we have studied the wireless communication systems, which is aided by the UAV with practical propulsion energy constraint consumed at the UAV. For both the minimum average rate maximization problem and the EE maximization problem, the UAV trajectories and the uplink transmit power of the GNs have been jointly optimized. Based on the SCA technique, we have proposed efficient iterative algorithms which find locally optimal solutions. From the numerical results, it can be demonstrated that the performance of the proposed algorithms provide substantial gains over the baseline schemes. As a future work, it would be interesting to investigate mobile GNs which changes their locations in each time slot. To this end, online trajectory optimization frameworks for the UAV may be essential. Moreover, optimizing the UAV trajectory with a more complicated model for movement and propulsion power consumption reflecting the mechanical characteristics of the UAV is worth pursuing. Also, the test-bed investigation and real-world implementation of the proposed UAV networks could be an important research direction.

## APPENDIX A
## PROOF OF LEMMA 1

First, we can define a function $f_1(\mathbf{u}) \triangleq \frac{1}{\rho\|\mathbf{u}\|^2+z}$ for $\mathbf{u} = [u_x\ u_y]^\intercal$ where $z$ and $\rho$ are positive constants. For any given $\mathbf{u}_l \in \mathbb{R}^{2\times 1}$, in order for arbitrary function $g_1(\mathbf{u}|\mathbf{u}_l)$ to be a concave surrogate function of $f_1(\mathbf{u})$, it must satisfy the following conditions: $f_1(\mathbf{u}_l) = g_1(\mathbf{u}_l|\mathbf{u}_l)$, $\nabla g_1(\mathbf{u}_l|\mathbf{u}_l) = \nabla f_1(\mathbf{u}_l)$, and $g_1(\mathbf{u}|\mathbf{u}_l) \leq f_1(\mathbf{u}), \quad \forall \mathbf{u}$ [26], [27]. Denoting the function $g_1(\mathbf{u}|\mathbf{u}_l)$ as

$$g_1(\mathbf{u}|\mathbf{u}_l) \triangleq -\frac{\rho\|\mathbf{u}\|^2}{z^2} + \overline{B}\mathbf{u}^\intercal\mathbf{u}_l + \overline{C}, \tag{42}$$

where $\overline{B} \triangleq 2\rho(\frac{1}{z^2} - \frac{1}{(\rho\|\mathbf{u}_l\|^2+z)^2})$ and $\overline{C} \triangleq \frac{1}{\rho\|\mathbf{u}_l\|^2+z} + \frac{2\rho\|\mathbf{u}_l\|^2}{(\rho\|\mathbf{u}_l\|^2+z)^2} - \frac{\rho\|\mathbf{u}_l\|^2}{z^2}$. It can be easily shown that $f_1(\mathbf{u}_l) = g_1(\mathbf{u}_l|\mathbf{u}_l)$, i.e., $g_1(\mathbf{u}|\mathbf{u}_l)$ fulfills the first condition for the surrogate function.

In addition, the gradient of $f_1(\mathbf{u})$ and $g_1(\mathbf{u}|\mathbf{u}_l)$ with respect to $\mathbf{u}$ can be derived as

$$\nabla f_1(\mathbf{u}) = -\frac{2\rho\mathbf{u}}{(\rho\|\mathbf{u}\|^2 + z)^2}, \tag{43}$$

$$\nabla g_1(\mathbf{u}|\mathbf{u}_l) = -\frac{2\rho\mathbf{u}}{z^2} + \overline{B}\mathbf{u}_l. \tag{44}$$

Since gradients in (43) and (44) hold equality at $\mathbf{u} = \mathbf{u}_l$, $g_1(\mathbf{u}|\mathbf{u}_l)$ satisfies the second condition for the surrogate function.

For proving the global lower bound condition, we can calculate the Hessian matrix $\nabla^2_{\mathbf{u}} h_1(\mathbf{u}|\mathbf{u}_l)$ of the function $h_1(\mathbf{u}|\mathbf{u}_l) \triangleq f_1(\mathbf{u}) - g_1(\mathbf{u}|\mathbf{u}_l)$ as

$$\nabla^2 h_1(\mathbf{u}|\mathbf{u}_l) = D \begin{bmatrix} E + 4\rho z^2 u_x^2 & 4\rho z^2 u_x u_y \\ 4\rho z^2 u_x u_y & E + 4\rho z^2 u_y^2 \end{bmatrix}, \qquad (45)$$

where $D \triangleq \frac{2\rho}{z^2(\rho\|\mathbf{u}\|^2 + z)^3} > 0$ and $E \triangleq \rho^3\|\mathbf{u}\|^6 + 3\rho^2 z\|\mathbf{u}\|^4 + 2\rho z^2\|\mathbf{u}\|^2 \geq 0$. It can be shown that the Hessian in (45) is a positive semi-definite matrix, which means that $h_1(\mathbf{u}|\mathbf{u}_l)$ is a convex function.

Because of $\nabla h_1(\mathbf{u}|\mathbf{u}_l) = \mathbf{0}$ at $\mathbf{u} = \mathbf{u}_l$ from (43) and (44), the global minimum of $h_1(\mathbf{u}|\mathbf{u}_l)$ is obtained at $\mathbf{u} = \mathbf{u}_l$ with $h_1(\mathbf{u}_l|\mathbf{u}_l) = 0$. As a result, we can show that $h_1(\mathbf{u}|\mathbf{u}_l)$ is greater than or equal to 0 for any given $\mathbf{u}_l$. Therefore, the third condition for the surrogate function holds. By substituting $\mathbf{u} = \mathbf{q}_{l+1}[n] - \mathbf{w}_k$, $\mathbf{u}_l = \mathbf{q}_l[n] - \mathbf{w}_k$, $z = H^2$, and $\rho = 1$ and multiplying $f_1(\mathbf{u})$ and $g_1(\mathbf{u}|\mathbf{u}_l)$ by $P_{\text{peak}}\gamma_0$, Lemma 1 is thus proved.

## REFERENCES


[1] S. Eom, H. Lee, J. Park, and I. Lee, "UAV-aided wireless communication design with propulsion energy constraint," in *Proc. IEEE Int. Conf. Commun.*, May 2018, pp. 1–6.

[2] Y. Zeng, R. Zhang, and T. J. Lim, "Wireless communications with unmanned aerial vehicles: Opportunities and challenges," *IEEE Commun. Mag.*, vol. 54, no. 5, pp. 36–42, May 2016.

[3] N. H. Motlagh, T. Taleb, and O. Arouk, "Low-altitude unmanned aerial vehicles-based internet of things services: Comprehensive survey and future perspectives," *IEEE Internet Things J.*, vol. 3, no. 6, pp. 899–922, Dec. 2016.

[4] W. Lee, I. Lee, J. S. Kwak, B.-C. Ihm, and S. Han, "Multi-BS MIMO cooperation: Challenges and practical solutions in 4G systems," *IEEE Wireless Commun.*, vol. 19, no. 1, pp. 89–96, Feb. 2012.

[5] X. Lin *et al.*, "The sky is not the limit: LTE for unmanned aerial vehicles," *IEEE Commun. Mag.*, vol. 56, no. 4, pp. 204–210, Apr. 2018.

[6] S. U. Rahman, G.-H. Kim, Y.-Z. Cho, and A. Khan, "Positioning of UAVs for throughput maximization in software-defined disaster area UAV communication networks," *J. Commun. Netw.*, vol. 20, pp. 452–463, Oct. 2018.

[7] H. Liu, S.-J. Yoo, and K. S. Kwak, "Opportunistic relaying for low-altitude UAV swarm secure communications with multiple eavesdroppers," *J. Commun. Netw.*, vol. 20, pp. 496–508, Oct. 2018.

[8] Y. Zeng, R. Zhang, and T. J. Lim, "Throughput maximization for UAV-enabled mobile relaying systems," *IEEE Trans. Commun.*, vol. 64, no. 12, pp. 4983–4996, Dec. 2016.

[9] Q. Wang, Z. Chen, W. Mei, and J. Fang, "Improving physical layer security using UAV-enabled mobile relaying," *IEEE Wireless Commun. Lett.*, vol. 6, no. 3, pp. 310–313, Jun. 2017.

[10] C. Song, K.-J. Lee, and I. Lee, "Designs of MIMO amplify-and-forward wireless relaying networks: Challenges and solutions," *IEEE Access*, vol. 5, pp. 9223–9234, May 2017.

[11] H.-B. Kong, C. Song, H. Park, and I. Lee, "A new beamforming design for MIMO AF relaying systems with direct link," *IEEE Trans. Commun.*, vol. 62, no. 7, pp. 2286–2295, Jul. 2014.

[12] A. Merwaday and I. Guvenc, "UAV assisted heterogeneous networks for public safety communications," in *Proc. IEEE Wireless Commun. Netw. Conf. Workshops*, May 2015, pp. 329–334.

[13] J. Lyu, Y. Zeng, and R. Zhang, "Spectrum sharing and cyclical multiple access in UAV-aided cellular offloading," in *Proc. IEEE GLOBECOM*, Dec. 2017, pp. 1–6.

[14] S. Jeong, O. Simeone, and J. Kang, "Mobile edge computing via a UAV-Mounted Cloudlet: Optimization of bit allocation and path planning," *IEEE Trans. Veh. Technol.*, vol. 67, no. 3, pp. 2049–2063, Mar. 2018.

[15] A. Al-Hourani, S. Kandeepan, and S. Lardner, "Optimal LAP altitude for maximum coverage," *IEEE Wireless Commun. Lett.*, vol. 3, no. 6, pp. 569–572, Jul. 2014.

[16] J. Lyu, Y. Zeng, and R. Zhang, "Cyclical multiple access in UAV-aided communications: A throughput-delay tradeoff," *IEEE Wireless Commun. Lett.*, vol. 5, no. 6, pp. 600–603, Dec. 2016.

[17] Q. Wu, Y. Zeng, and R. Zhang, "Joint trajectory and communication design for multi-UAV enabled wireless networks," *IEEE Trans. Wireless Commun.*, vol. 17, no. 3, pp. 2109–2121, Apr. 2018.

[18] A. Filippone, *Flight Performance of Fixed and Rotary Wing Aircraft*. New York, NY, USA: Elsevier, 2006.

[19] D. H. Choi, S. H. Kim, and D. K. Sung, "Energy-efficient maneuvering and communication of a single UAV-based relay," *IEEE Trans. Aerosp. Electron. Syst.*, vol. 50, no. 3, pp. 2320–2327, Jul. 2014.

[20] J. Zhang, Y. Zeng, and R. Zhang, "Spectrum and energy efficiency maximization in UAV-enabled mobile relaying," in *Proc. IEEE Int. Conf. Commun.*, May 2017, pp. 1–6.

[21] Y. Zeng and R. Zhang, "Energy-efficient UAV communication with trajectory optimization," *IEEE Trans. Wireless Commun.*, vol. 16, no. 6, pp. 3747–3760, Jun. 2017.

[22] J. Xu and L. Qiu, "Energy efficiency optimization for MIMO broadcast channels," *IEEE Trans. Wireless Commun.*, vol. 12, no. 2, pp. 690–701, Feb. 2013.

[23] S.-R. Lee, J. Jung, H. Park, and I. Lee, "A new energy-efficient beamforming strategy for MISO interfering broadcast channels based on large systems analysis," *IEEE Trans. Wireless Commun.*, vol. 15, no. 4, pp. 2872–2882, Apr. 2016.

[24] L. Zhang, Y.-C. Liang, and Y. Xin, "Joint beamforming and power allocation for multiple access channels in cognitive radio networks," *IEEE J. Sel. Areas Commun.*, vol. 26, no. 1, pp. 38–51, Sep. 2008.

[25] N. Zhang, J. Wang, G. Kang, and Y. Liu, "Uplink nonorthogonal multiple access in 5G systems," *IEEE Commun. Lett.*, vol. 20, no. 3, pp. 458–461, Mar. 2016.

[26] M. Razaviyayn, "Successive convex approximation: Analysis and applications," Ph.D. dissertation, Univ. Minnesota, Minneapolis, MN, USA, 2014.

[27] B. R. Marks and G. P. Wright, "A general inner approximation algorithm for nonconvex mathematical programs," *Oper. Res.*, vol. 26, pp. 681–683, Aug. 1978.

[28] B. Du, C. Pan, W. Zhang, and M. Chen, "Distributed energy-efficient power optimization for CoMP systems with max-min fairness," *IEEE Commun. Lett.*, vol. 18, no. 6, pp. 999–1002, Jun. 2014.

[29] Y. Li *et al.*, "Energy-efficient subcarrier assignment and power allocation in OFDMA systems with max-min fairness guarantees," *IEEE Trans. Commun.*, vol. 63, no. 6, pp. 3183–3195, Sep. 2015.

[30] S. Boyd and L. Vandenberghe, *Convex Optimization*. Cambridge, U.K.: Cambridge Univ. Press, 2004.

[31] M. Grant and S. Boyd, "CVX: Matlab software for disciplined convex programming, version 2.1," 2017. [Online]. Available: http://cvxr.com/cvx

[32] W. Dinkelbach, "On nonlinear fractional programming," *Manag. Sci.*, vol. 13, pp. 492–498, Mar. 1967.

[33] A. Zappone and E. Jorswieck, "Energy efficiency in wireless networks via fractional programming theory," *Found. Trends Commun. Inf. Theory*, vol. 11, pp. 185–396, Jun. 2015.


**Subin Eom** received the B.S. and M.S. degrees in electrical engineering from Korea University, Seoul, South Korea, in 2015 and 2017, respectively. He is currently working toward the Ph.D. degree with the School of Electrical Engineering, Korea University. His research interests include information theory and optimization for the next-generation wireless communications such as UAV-enabled wireless networks and mobile edge computation networks.

**Hoon Lee** (S'14-M'18) received the B.S. and Ph.D. degrees in electrical engineering from Korea University, Seoul, South Korea, in 2012 and 2017, respectively. In 2015, he visited Imperial College London, London, U.K., to conduct a collaborative research. In 2017 and 2018, he was a Postdoctoral Fellow with Korea University, and Singapore University of Technology and Design, Singapore, respectively. Since 2019, he has been with Pukyong National University, Busan, South Korea, where he is currently an Assistant Professor with the Department of Information and Communication Engineering. His research interests include machine learning and signal processing for wireless communications such as visible light communications, wireless energy transfer communication systems, and secure wireless networks.

**Junhee Park** received the B.S. and M.S. degrees in electrical engineering from Korea University, Seoul, South Korea, in 2015 and 2017, respectively. He is currently working toward the Ph.D. degree with the School of Electrical Engineering, Korea University. His research interests include signal processing and information theory for the next-generation wireless communications such as UAV-enabled wireless networks and energy harvesting communication systems.

**Inkyu Lee** (S'92–M'95–SM'01–F'16) received the B.S. (Hons.) degree in control and instrumentation engineering from Seoul National University, Seoul, South Korea, in 1990, and the M.S. and Ph.D. degrees in electrical engineering from Stanford University, Stanford, CA, USA, in 1992 and 1995, respectively. From 1995 to 2001, he was a Member of the Technical Staff with Bell Laboratories, Lucent Technologies, where he studied high-speed wireless system designs. From 2001 to 2002, he was a Distinguished Member of the Technical Staff with Agere Systems (formerly the Microelectronics Group, Lucent Technologies), Murray Hill, NJ, USA. Since 2002, he has been with Korea University, Seoul, South Korea, where he is currently a Department Head of the School of Electrical Engineering. In 2009, he was a Visiting Professor with the University of Southern California, Los Angeles, CA. He has authored or coauthored more than 180 journal papers in IEEE publications and has 30 U.S. patents granted or pending. His research interests include digital communications, signal processing, and coding techniques applied for next-generation wireless systems. Dr. Lee has served as an Associate Editor for the IEEE TRANSACTIONS ON COMMUNICATIONS from 2001 to 2011 and the IEEE TRANSACTIONS ON WIRELESS COMMUNICATIONS from 2007 to 2011. In addition, he was a Chief Guest Editor for the IEEE JOURNAL ON SELECTED AREAS IN COMMUNICATIONS (Special Issue on 4 G Wireless Systems) in 2006. He currently serves as a Co-Editor-in-Chief for the *Journal of Communications and Networks*. He was a recipient of the IT Young Engineer Award at the IEEE/IEEK Joint Award in 2006 and of the Best Paper Award at the Asia-Pacific Conference on Communications in 2006, the IEEE Vehicular Technology Conference in 2009, and the IEEE International Symposium on Intelligent Signal Processing and Communication Systems in 2013. He was also a recipient of the Best Research Award from the Korean Institute of Communications and Information Sciences (KICS) in 2011, the Best Young Engineer Award from the National Academy of Engineering in Korea in 2013, and the Korea Engineering Award from the National Research Foundation of Korea in 2017. He has been elected as a member of National Academy of Engineering in Korea in 2015, and is an IEEE Distinguished Lecturer.